Journal of Radioanalytical and Nuclear Chemistry (2022) 331:1859–1867
https://doi.org/10.1007/s10967-022-08250-z

A comparative investigation of uranium and thorium adsorption behavior on amidoximated copolymeric hydrogel

Zeinab F. Akl[1]

Received: 17 January 2022 / Accepted: 21 February 2022 / Published online: 25 March 2022
© The Author(s) 2022

Abstract
This work focuses on investigating the feasibility of using a crosslinked amidoximated copolymeric hydrogel as a potential adsorbent to recover uranium and thorium ions from aqueous media. The hydrogel was synthesized via gamma-irradiation copolymerization and characterized through FTIR, TGA, and SEM. The medium acidity notably affected the adsorption capacity of both ions. The adsorption data was in line with the pseudo-1st-order equation and the Freundlich isothermal model. The thermodynamics analysis showed that the temperature rise promoted the adsorption capacity. The reusability studies highlighted the good performance of the hydrogel up to five regeneration rounds.

Keywords Chelating polymers · γ-Induced copolymerization · Uranium · Thorium · Recovery

Introduction

The interest in uranium and thorium has expanded tremendously, due to their technological importance and considerable benefits in a number of fields including nuclear power, medical, agricultural, industrial, and defense applications [1]. Uranium and thorium are naturally occurring radionuclides found mainly in rocks, sands, and aquatic environments [2]. Their recovery from mineral ores is achieved mainly via ion-exchange and solvent extraction; after various ore preconcentration and leaching processes [3]. In nature, thorium is found as a tetravalent cation, whereas uranium is found in both tetravalent and hexavalent states. In aqueous solutions, thorium is only stable at the tetravalent form [4], whereas hexavalent uranium is the more stable form. Uranium and thorium behavior, content, and speciation in the aqueous solutions are complicated and controlled by the pH [5].

The reserve of uranium and thorium is estimated to be around 7 and 10 million tons, respectively [6]. Due to the anticipated uranium and thorium shortage, their recovery from unconventional resources, such as natural waters, seawater, industrial wastewaters, and other waste sources, became a significant task for the sustainable development of nuclear energy [7]. Besides, the radioactive and toxic nature of these radionuclides made their removal and recovery from the contaminated waters essential to minimize their discharge into the environment [8]. To date, numerous techniques have been applied for uranium and thorium separation, recovery, and removal such as chemical precipitation, electrochemical treatment, flotation, adsorption, ion-exchange, biodegradation, chromatographic extraction, photocatalysis, solvent extraction, and membrane technologies [6, 9–15]. Recently, attention has been increased to the adsorption technique for economic and effective extraction of radionuclides from water media, due to its reliability, feasibility, ease of handling, fast kinetics, and the adsorbent reusability [16, 17].

The adsorption technique retains the radionuclides via establishing adsorbate–adsorbent equilibrium through different mechanisms as ion exchange, chelation, complexation, and electrostatic interactions [18]. Many efforts are diverted to developing effective adsorbents with elevated adsorption capacity, selectivity, and irradiation stability [19]. Various organic, inorganic, or composite adsorbents have been developed for uranium and thorium recovery including synthetic polymers [20], silicon materials [21], carbon-based materials [22], clay minerals [23], resins [24], cellulose [25], metal-organic frameworks [26], and chitosan-based adsorbents [27].

✉ Zeinab F. Akl
eltasneem2007@yahoo.com

[1] Egyptian Atomic Energy Authority, P.O. Box 11762, Cairo, Egypt

Over the recent decades, the functionalized chelating polymers have received significant interest in radioactive waste separation thanks to their advantages such as raised performance, cost-effectiveness, and simplicity of surface modification [28]. Particularly, amidoxime-functionalized polymers are excellent adsorbents for uranium and thorium capture from aquatic media owing to their high efficiency, elevated selectivity, and fast kinetics [29]. Amidoximes have outstanding functionality via the joint possession of acidic (–OH) and basic ($–NH_2$) active sites which can effectively bind uranium and thorium ions. Amidoxime-based adsorbents showed high-performance thanks to their superb chemical activity and excellent adsorption ability.

Efficient chelating polymers can be developed through the copolymerization of monomers having different functional groups. The introduction of hydrophilic groups, e.g. carboxylic or sulfonic, was reported to enhance the adsorption capacity of the amidoximated adsorbents [30]. In this view, this work aims at exploring the adsorption behavior of the crosslinked amidoximated hydrogel towards uranium and thorium ions. The parameters that affect the adsorption process were investigated and optimized. The adsorption rate and capacity were analyzed through the application of linear forms of various kinetics and isotherms models.

Experimental

Reagents and instruments

Analytical grade chemicals and deionized water were used in the experimental work. Acrylonitrile (AN) and arsenazo-III were obtained from Sigma-Aldrich (Germany). Hydroxylamine hydrochloride and 2-acrylamido-2-methylpropane sulfonic acid (AMPS) were supplied by Merck (Germany). *N*,*N*′-Methylenebisacrylamide (MBA) was purchased from Thermo Fisher Scientific (USA). U(VI) and Th(IV) solutions were acquired via dissolving an accurately weighed amount of the corresponding nitrate form in deionized water.

The hydrogel chemical composition was identified by FTIR (Nicolet iS10 spectrophotometer, Thermo Scientific, Japan). The hydrogel surface features were analyzed through SEM (JEOL-6510 LA, Japan). The hydrogel thermal stability was investigated via TGA (Shimadzu TGA-50, Japan) within the temperature range 25–650 °C at heating and nitrogen flow rates of 10 °C min^{-1} and 20 mL min^{-1}, respectively. U(VI) and Th(IV) concentrations were measured by UV–Vis spectrophotometer (Thermo evolution 300, UK).

Preparation and amidoximation of the hydrogel

AN/AMPS crosslinked copolymeric hydrogel was prepared by means of gamma irradiation-induced free radical copolymerization technique. The monomers having a 70/30 feed composition (AN/AMPS) were dissolved in deionized water in the presence of 0.25 wt% of MBA and then purged with nitrogen for 10 min. At that point, the solution was subjected to γ-rays from ^{60}Co source at a radiation dose of 30 kGy. The irradiated copolymer was chopped into pieces, rinsed with methanol followed by deionized water, and then kept at 60 °C overnight.

The amidoximation reaction was carried out by adding methanolic hydroxylamine solution to the synthesized copolymer (AN/AMPS) followed by heating at 70 °C for 3 h under constant stirring conditions. The amidoximated copolymer (AO/AMPS) was filtered, rinsed with deionized water, and dried overnight at 60 °C.

Adsorption experiments

The adsorption experiments were conducted using the single-component batch-wise technique. The adsorption process was accomplished via agitation of conical flasks, containing a constant amount of the hydrogel and aqueous solutions of each radionuclide, for a given time using a thermostatically controlled shaking bath. After filtration, the remaining quantity of each ion was evaluated spectrophotometrically [31].

The relation between the hydrogel performance and the experimental variables, including solution pH (2 – 8), radionuclide quantity (50 – 500 mg/l), contact time (0 – 220 min), and solution temperature (30 – 60 °C), was investigated.

The equilibrium adsorption capacity of the AO/AMPS copolymeric hydrogel (q_e, mg g^{-1}) was calculated using the following expression [32]:

$$q_e = \frac{(C_o - C_e)V}{W} \quad (1)$$

where C_o and C_e (mg L^{-1}) are the initial and equilibrium concentrations of each radionuclide, V (L) is the solution volume, and W (g) is the hydrogel mass.

Adsorption experiments were conducted in triplicate and the average values were reported.

Results and discussion

Structural characteristics of AO/AMPS hydrogel

Figure 1a, b shows the FTIR spectra of the prepared hydrogel before and after the amidoximation process, respectively. For AN/AMPS copolymer (Fig. 1a), the band at 2928 cm^{-1} represented the (CH_2) vibration in the copolymer chains. The (C–H) stretching vibration was observed at 2850 cm^{-1} [31]. The peak at 1729 cm^{-1} indicated the (C=O) stretching

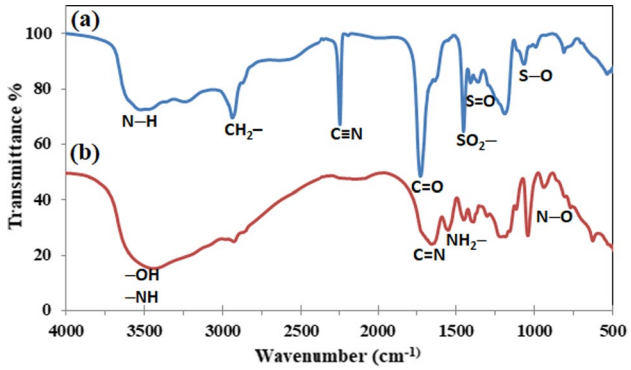

Fig. 1 FTIR graph of (**a**) AN/AMPS and (**b**) AO/AMPS copolymeric hydrogel

vibration from AMPS secondary amide group [33]. The vibration bands of the sulfonyl group appeared at 1066 cm^{-1} (S–O), 1360 cm^{-1} (S=O), and 1453 cm^{-1} (SO_2), respectively [31]. The sharp peak at 2243 cm^{-1} was assigned to the (C≡N) group, whereas the board peak at 3524 cm^{-1} was due to the (N–H) stretching [33]. The disappearance of the (C≡N) peak in the AO/AMPS spectrum (Fig. 1b) demonstrated the successful conversion of the cyano group to an amidoxime group. The new amidoxime group characteristic peaks appeared at 1658 cm^{-1} (C=N stretching), 939 cm^{-1} (N–O stretching), 1552 cm^{-1} (NH_2– bending) vibrations. The 3441 cm^{-1} broadband was belonged to the stretching vibration of the (–OH) overlapped with the (–NH) in the amidoxime group [31].

SEM was used to investigate the hydrogel microstructure morphology and give insights into the compatibility of the monomers. The AO/AMPS micrograph (Fig. 2) showed a uniform porous structure with numerous interconnected pores distributed on the hydrogel surface. The noticed capillary channels would allow the radionuclides and water molecules to enter into the hydrogel networks [34]. Additionally, the observed pores interconnection confirmed the crosslinked network structure and suggested the smooth flow of the radionuclides into the AO/AMPS hydrogel.

TGA was performed to assess the thermal stability and degradation profile of the AO/AMPS copolymeric hydrogel (Fig. 3). The TGA plot showed an initial decomposition stage that took place at 50–200 °C with approximately 10% mass loss that represented the evaporation of the absorbed and bound water. The subsequent degradation stage occurred in the range of 200–300 °C with an additional 10% mass loss; was assigned to the decomposition of AMPS sulfonic acid groups and production of sulfur oxide gases (SO_2 and SO_3) [35]. The next degradation stage appeared in the range of 300–350 °C with 20% mass loss and indicated the amide group decomposition [36]. The final stage was observed in the range of 350–550 °C with 35% mass loss which was due to the thermal degradation of the backbone chain.

pH–adsorption relationship

Figure 4 illustrates the variation of the adsorption capacity with the medium pH. The results indicated that the adsorption behavior was sensitive to the pH changes; as it was quantitative only within the pH range 3–5 for both radionuclides. Such behavior can be explained based on the hydrogel protonation–deprotonation process as well as the variation of the radionuclide species with the medium pH. The solution pH influenced the radionuclides hydrolysis and consequently the adsorption mechanism. At low pH values, the cationic UO_2(II) and Th(IV) species predominated in the solution and competed with the excess protons for the hydrogel active sites that eventually suppressed the adsorption capacity [37, 38]. Additionally, under high acidic conditions the sulfonic and oxime groups of AO/AMPS were protonated and consequently couldn't provide sufficient coordination sites for the radionuclides [39]. As the pH increased, the deprotonation

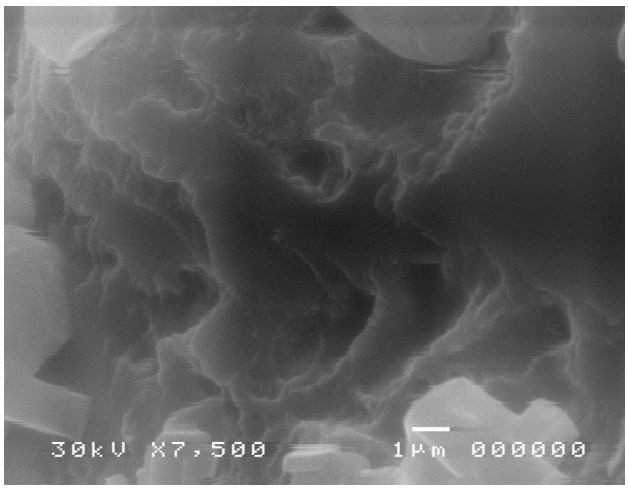

Fig. 2 SEM image of AO/AMPS copolymeric hydrogel

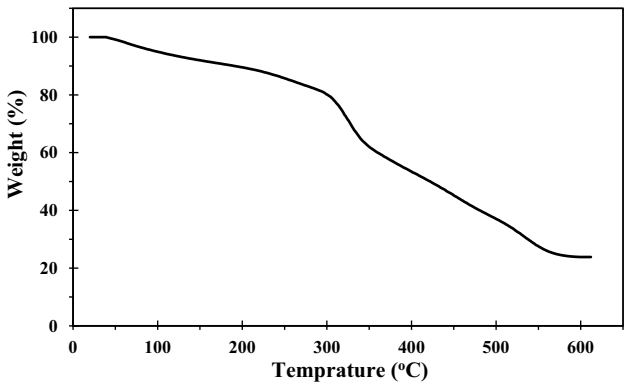

Fig. 3 TGA graph of AO/AMPS copolymeric hydrogel

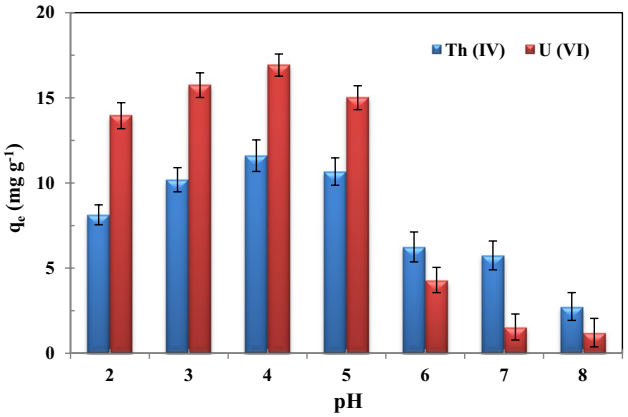

Fig. 4 pH–adsorption relationship for U(VI) and Th(IV) ions on AO/AMPS copolymeric hydrogel

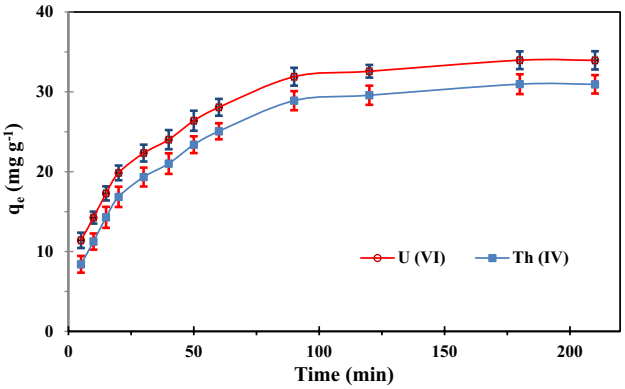

Fig. 5 Time–adsorption relationship for U(VI) and Th(IV) ions on AO/AMPS copolymeric hydrogel

of the oxime and sulfonic groups favored the radionuclides adsorption as more active sites were exposed to uranium and thorium, thereby increasing the adsorption capacity [40]. At further pH increment (pH > 4), U(VI) and Th(IV) hydrolysis and precipitation phenomena adversely affected the adsorption process [40] and consequently the adsorbed amount of the radionuclides fell off. Hence, pH 4 was used for further adsorption studies.

Time–adsorption relationship

The time required by the adsorbent to reach the adsorption equilibrium is of utmost importance when evaluating the adsorbent efficiency. The equilibrium time is dependent on the adsorbent nature and the adsorption mechanism; and should be optimized to set the optimal settings when designing a full-scale batch adsorption process. For this purpose, the influence of the contact time on the adsorption behavior was examined at pH 4 for different time intervals. According to Fig. 5, the adsorbed amount of both radionuclides increased quickly with contact time at the first stage (40 min); and thereafter it proceeded at a slower rate till the equilibrium was reached in 120 min.

In beginning, the observed fast increase of the radionuclide adsorbed quantity resulted from the enormous number of free binding sites on AO/AMPS copolymeric hydrogel, thus the radionuclides could migrate towards the boundary layer of the hydrogel surface, begin to occupy the free adsorption sites, and finally populate the interior sites of the porous construction via pore diffusion [41]. By increasing the contact time, the hydrogel binding sites were gradually saturated causing a slower adsorption rate until the equilibrium was attained and no further significant increase in the adsorption capacity was noticed. Based on the adsorption results, 120 min was considered as the appropriate time for further experiments.

Initial concentration–adsorption relationship

The adsorbate initial concentration is one of the most significant factors which can influence the adsorption behavior. In this regard, solutions with different concentrations of each individual radionuclide (50–500 mg L^{-1}) were equilibrated with AO/AMPS copolymeric hydrogel for 120 min at 25 °C and pH 4. Figure 6 shows the changing trend of the hydrogel adsorption capacity with the radionuclide concentration, which exhibited a gradual upward relationship until reaching a plateau.

At low initial concentrations, AO/AMPS copolymeric hydrogel had a relatively high number of free adsorption sites; thus, the ratio of the radionuclide ions to the accessible active sites was low. By increasing the radionuclide concentration, the active sites of AO/AMPS copolymer would be surrounded with more radionuclide ions leading to a stronger driving force that conquer the radionuclides mass-transfer

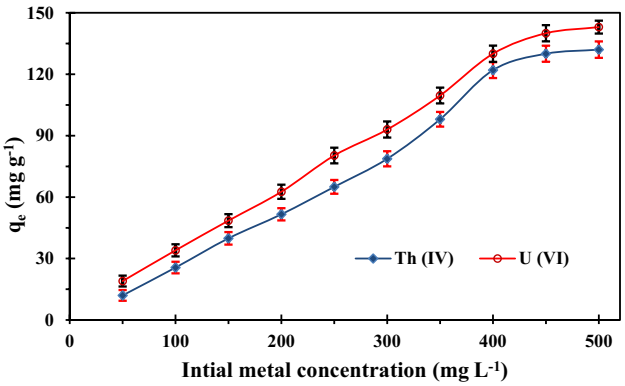

Fig. 6 Initial concentration–adsorption relationship for U(VI) and Th(IV) ions on AO/AMPS copolymeric hydrogel

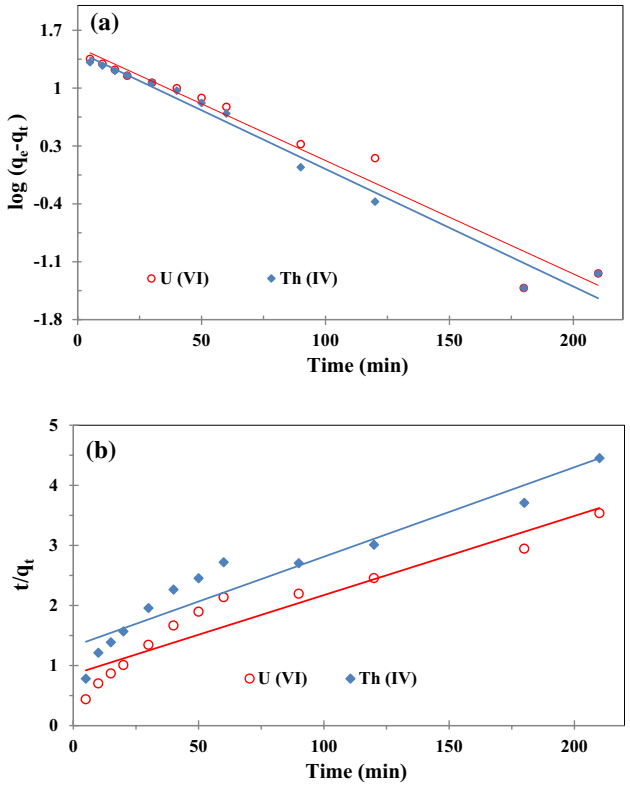

Fig. 7 Linear fitting plots of (**a**) pseudo-1st--order and (**b**) pseudo-2nd-order models for U(VI) and Th(IV) ions adsorption on AO/AMPS copolymeric hydrogel

limitations between the liquid and solid phases; and consequently better adsorption capacity was noticed till the binding sites were saturated [42].

Kinetics investigations

To gain an insight into the adsorption rate, determine the potential control-rate steps, and reveal the adsorption mechanism; the compatibility of the kinetics results to the pseudo-1st-order and pseudo-2nd-order reactions was evaluated. The success of the model in predicting the adsorption kinetics was indicated by a relatively high value of the correlation coefficients (R^2). The mathematical linear formulas of the studied kinetics models and the corresponding parameters for U(VI) and Th(IV) adsorption on AO/AMPS hydrogel were summarized in Table 1 and Fig. 7. The data showed that the pseudo-1st-order model had greater correlation coefficients for both radionuclides, which implies its better ability to describe the adsorption kinetics. Additionally, the values of q_e calculated by the pseudo-1st-order model agreed well with the experimental values (30.94 and 26.95 mg g^{-1} for U(VI) and Th(IV) ions, respectively). This observations suggested that the diffusion process was the rate-limiting step in the radionuclides adsorption.

Isotherms investigations

Adsorption isotherms analysis was performed to predict the AO/AMPS adsorption capacity, understand adsorbent-adsorbate interaction mechanism, and get information on the active sites' distribution on the surface of AO/AMPS hydrogel as well as the nature of coverage (monolayer or multilayer). The experimental results were fitted to Langmuir, Freundlich, and Temkin isotherms. Table 2 summarizes the isotherms linear equations, fitting parameters, and R^2 values; whereas Fig. 8 shows the corresponding linear relationship. The experimental data was more adequately described by the Freundlich model compared with other models, as was indicated from the higher R^2 values. This sugessted a heterogeneous adsorption surface due to the various functional groups on the AO/AMPS surface [43]. The calculated n values were higher than 1 for both radionuclides, pointing out a favorable adsorption process; while 1/*n* values were lower than 1, indicating a strong interaction between the radionuclides and AO/AMPS copolymeric hydrogel.

For the Langmuir model, the calculated maximum adsorption capacity q_{max} was 502.51 and 434.78 mg g^{-1} for U(VI) and Th(IV), respectively. The dimensionless separation factor (R_L) was utilized to describe the affinity of AO/AMPS active sites towards U(VI) and Th(IV) ions. The calculated R_L values were falls between 0 and 1 (0.44–0.86 and 0.64–0.94 for U(VI) and Th(IV), respectively), denoting a highly favorable adsorption process [44]. The results clearly indicated the suitability of AO/AMPS copolymeric

Table 1 Kinetic parameters for U(VI) and Th(IV) ions adsorption on AO/AMPS copolymeric hydrogel

Adsorption model name	Linear form	Parameter description	Value for U(VI)	Value for Th(IV)
Pseudo-1st-order	$log(q_e - q_t) = logq_e - \left(\frac{k_1}{2.303}\right)t$	q_e (mg g^{-1}) is the equilibrium adsorption capacity	31.30	27.66
		K_1 (min^{-1}) is the adsorption rate constant	0.031	0.032
		R^2 is the correlation coefficient	0.974	0.986
Pseudo-2nd-order	$\frac{t}{q_t} = \frac{1}{k_2 q_e^2} + \frac{1}{q_e}t$	q_e (mg g^{-1}) is the equilibrium adsorption capacity	75.75	67.11
		K_2 (g mg^{-1} min^{-1}) is the adsorption rate constant	0.015	0.011
		R^2 is the correlation coefficient	0.903	0.909

Table 2 Isotherm parameters for U(VI) and Th(IV) ions adsorption on AO/AMPS copolymeric hydrogel

Adsorption model name	Linear form	Parameter description	Value for U(VI)	Value for Th(IV)
Langmuir isotherm model	$\frac{C_e}{q_e} = \frac{C_e}{q_{max}} + \frac{1}{q_{max} K_L}$	q_{max} (mg g^{-1}) is the maximal adsorption capacity	502.51	434.78
		K_L (L mg^{-1}) is Langmuir constant	0.004	0.003
		R^2 is the correlation coefficient	0.898	0.896
		R_L is the separation factor $R_L = \frac{1}{1+K_L C_o}$	0.033–0.255	0.086–0.431
Freundlich isotherm model	$\log q_e = \log k_F + \frac{1}{n} \log C_e$	K_F (mg g^{-1}) is Freundlich constant	2.10	1.24
		n (L g^{-1}) is the adsorption intensity	1.30	1.03
		R^2 is the correlation coefficient	0.993	0.991
Temkin isotherm model	$q_e = B \ln A_T + B \ln C_e$	b_T (J mol^{-1}) is Temkin constant	50.94	50.15
		A_T (L g^{-1}) is the equilibrium binding constant	13.13	7.84
		R^2 is the correlation coefficient	0.942	0.938

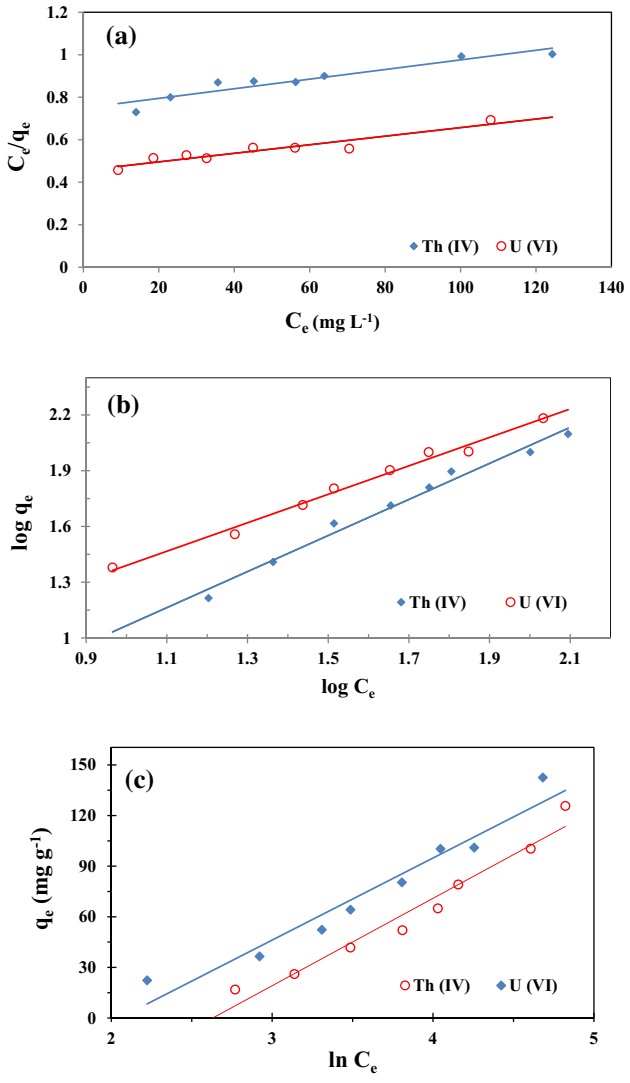

Fig. 8 Linear fitting plots of (**a**) Langmuir, (**b**) Freundlich, and (**c**) Temkin isotherms for U(VI) and Th(IV) ions adsorption on AO/AMPS copolymeric hydrogel

hydrogel for U(VI) and Th(IV) adsorptive recovery from water streams.

Thermodynamics investigations

To foresee the temperature–adsorption relationship, the U(VI) and Th(IV) adsorption on AO/AMPS copolymeric hydrogel was studied under the temperature range 30–60 °C. The corresponding results revealed an enhancement of the adsorption ability with the temperature increase, indicating the endothermic nature of the adsorption reaction. This can be explained as that, at higher temperatures the intraparticle diffusion increased and more adsorption sites were available which boost up the adsorption phenomenon.

To fully understand the adsorption nature and predict the adsorption spontaneity, thermodynamics analysis was performed and the correlating parameters were estimated based on the equations listed in Table 3 as well as the Van't Hoff plot (Fig. 9). Data given in Table 3 confirmed the endothermic nature of the adsorption reaction, as indicated from the positive value of the standard enthalpy (ΔH°). Moreover, the high enthalpy value ($\Delta H^\circ > 40\,kJ\,mol^{-1}$) indicated a chemisorption process. Results showed negative values for the standard free energy (ΔG°) reflecting the adsorption spontaneity and feasibility. Lower ΔG° values were observed for higher temperatures, signifying better adsorption capacity at elevated temperatures. The positive charge of the standard entropy (ΔS°) reflected the affinity of AO/AMPS hydrogel towards the tested radionuclides. Additionally, ΔS° values suggested a potential higher randomness at the hydrogel/solution interface during U(VI) and Th(IV) adsorption [45].

Reusability of AO/AMPS copolymer

From the environmental, economic, and industrial viewpoint; good regeneration and reusability are highly required for materials applied to pollutants removal. This is to lower the adsorption process cost and avoid the accumulation of

Table 3 Thermodynamic parameters for U(VI) and Th(IV) ions adsorption on AO/AMPS copolymeric hydrogel

Parameter	ΔH° (kJ mol^{-1})	ΔS° (J mol^{-1} K^{-1})	ΔG° (kJ mol^{-1})				
Formula	$lnK_c = -\frac{\Delta H^o}{RT} + \frac{\Delta S^o}{R}$ $K_c = \frac{q_e}{C_e}$	$\Delta S^o = \frac{\Delta H^o - \Delta G^o}{T}$	$\Delta G^o = -RTlnK_c$				
				Temperature (K)			
				303.15	313.15	323.15	333.15
Value for U(VI)	42.20	135.59	− 1.41	− 2.69	− 3.99	− 5.49	
Value for Th(IV)	41.26	133.03	− 0.129	− 1.29	− 2.67	− 4.11	

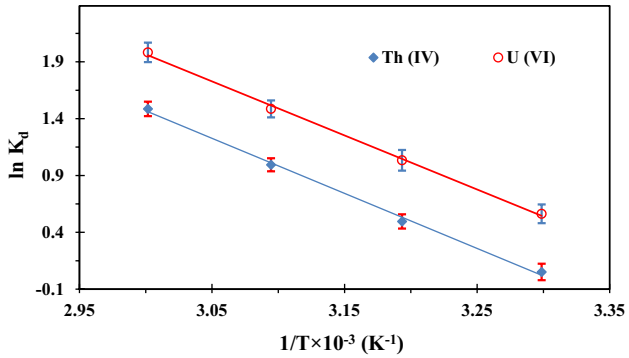

Fig. 9 Van't Hoff plots for U(VI) and Th(IV) ions adsorption on AO/AMPS copolymeric hydrogel

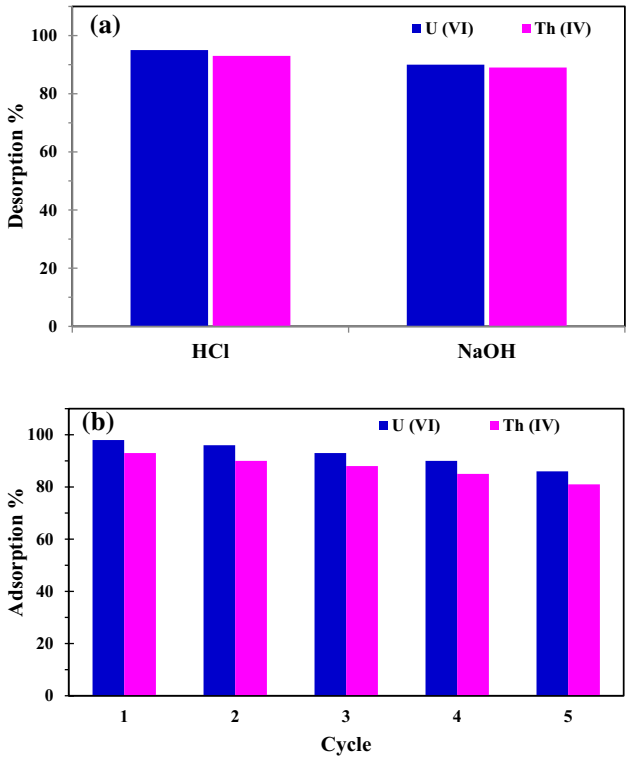

Fig. 10 Desorption (**a**) and reusability (**b**) of AO/AMPS copolymeric hydrogel

pollutant-loaded materials in the environment. Therefore, the desorption of loaded-AO/AMPS copolymeric hydrogel was investigated using HCl and NaOH solutions (1 mol L^{-1}). Figure 10a showed higher desorption percentages of both radionuclides in the acidic medium than in the basic medium. U(VI) ions were eluted close to 95% by HCl and 90% by NaOH, while Th(IV) ions were eluted close to 94% by HCl and 89% by NaOH.

The regenerated copolymeric hydrogel was applied for five successive adsorption–desorption cycles. The results indicated

that the first round had the highest removal efficiency due to the intact pores and binding sites. Although the adsorption capacity gradually decreased after each successive round of reuse, the efficacy of the adsorption remained relatively high after the fifth round. This finding confirmed that AO/AMPS copolymeric hydrogel had good reusability and stability for U(VI) and Th(IV) recovery from the aquatic environments.

Conclusions

Amidoxime-based chelating copolymeric hydrogel has been synthesized, characterized, and successfully applied as an efficient candidate for U(VI) and Th(IV) adsorptive recovery. The pH and kinetics studies designated pH 4 and 120 min as the optimal values for maximum adsorption capacity. The amidoximated hydrogel revealed a higher adsorption capacity toward U(VI) (502.51 mg g^{-1}) than Th(IV) (434.78 mg g^{-1}). Thermodynamics results indicated the endothermic and spontaneous characteristics of U(VI) and Th(IV) adsorption on AO/AMPS hydrogel. Desorption of the radionuclides from the AO/AMPS hydrogel was realized by using 1 mol L^{-1}HCl. The adsorbent showed remarkable adsorption capacity, high regeneration capability, good stability, and fast equilibrium time indicating its potential practicability for large-scale treatment of uranium and thorium contaminated water streams.

Funding Open access funding provided by The Science, Technology & Innovation Funding Authority (STDF) in cooperation with The Egyptian Knowledge Bank (EKB).

Declarations

Conflict of interest The author declares that there is no conflict of interest.

Open Access This article is licensed under a Creative Commons Attribution 4.0 International License, which permits use, sharing, adaptation, distribution and reproduction in any medium or format, as long as you give appropriate credit to the original author(s) and the source, provide a link to the Creative Commons licence, and indicate if changes were made. The images or other third party material in this article are included in the article's Creative Commons licence, unless indicated otherwise in a credit line to the material. If material is not included in the article's Creative Commons licence and your intended use is not permitted by statutory regulation or exceeds the permitted use, you will need to obtain permission directly from the copyright holder. To view a copy of this licence, visit http://creativecommons.org/licenses/by/4.0/.

References

1. Shelar-Lohar G, Joshi S (2019) Comparative study of uranium and thorium metal ion adsorption by gum ghatti grafted poly(acrylamide) copolymer composites. RSC Adv 9:41326–41335. https://doi.org/10.1039/C9RA08212C
2. Yakout SM, Abdeltawab AA (2015) Adsorption of uranium in the presence of different ions, humic acid and effect of thorium on uranium adsorption by activated carbon. Desalin Water Treat 55:2209–2220. https://doi.org/10.1080/19443994.2014.937757
3. El-Nadi YA, Daoud JA (2005) Sorption of uranium and thorium from sulphuric acid using TVEX-PHOR resin. J Radioanal Nucl Chem 265:447–454. https://doi.org/10.1007/s10967-005-0847-x
4. Erden KE, Donat R (2017) Removal of thorium (IV) from aqueous solutions by natural sepiolite. Radiochim Acta 105:187–196. https://doi.org/10.1515/ract-2016-2667
5. Xiong J, Hu S, Liu Y, Yu J, Yu H, Xie L, Wen J, Wang X (2017) Polypropylene modified with amidoxime/carboxyl groups in separating uranium(VI) from thorium(IV) in aqueous solutions. ACS Sustain Chem Eng 5:1924–1930. https://doi.org/10.1021/acssuschemeng.6b02663
6. Aziman ES, Salehuddin AHJM, Ismail AF (2021) Remediation of thorium (IV) from wastewater: Current status and way forward. Sep Purif Rev 50:177–202. https://doi.org/10.1080/15422119.2019.1639519
7. Whitty-Léveilléa L, Aumaitre C, Morin JF, Reynie N, Larivière D (2019) Design of an adsorbent-bearing silica Schiff base ligand for the highly efficient removal of uranium and thorium in acidic solutions. Sep Purif Technol 228:115709. https://doi.org/10.1016/j.seppur.2019.115709
8. Wang Y, Hu X, Liu Y, Li Y, Lan T, Wang C, Liu Y, Yuan D, Cao X, He H, Zhou L, Liu Z, Chew JW (2021) Assembly of three-dimensional ultralight poly(amidoxime)/graphene oxide nanoribbons aerogel for efficient removal of uranium(VI) from water samples. Sci Total Environ 765:142686. https://doi.org/10.1016/j.scitotenv.2020.142686
9. Tyrpekl V, Beliš M, Wangle T, Vleugels J, Verwerft M (2017) Alterations of thorium oxalate morphology by changing elementary precipitation conditions. J Nucl Mater 493:255–263. https://doi.org/10.1016/j.jnucmat.2017.06.027
10. Amphlett JTM, Choi S, Parry SA, Moon EM, Sharrad CA, Ogden MD (2020) Insights on uranium uptake mechanisms by ion exchange resins with chelating functionalities: Chelation vs. anion exchange. Chem Eng J 392:123712. https://doi.org/10.1016/j.cej.2019.123712
11. Ghoniemy EA, Mohammaden TF, El-Shahat MR, Elkhawaga MA, Rezk MM, Wessam MM (2020) Fungal treatment for liquid waste containing U(VI) and Th(IV). Biotechnol Rep 26:e00472. https://doi.org/10.1016/j.btre.2020.e00472
12. Hurtado-Bermúdez S, Villa-Alfageme M, Mas JL, Alba MD (2018) Comparison of solvent extraction and extraction chromatography resin techniques for uranium isotopic characterization in high-level radioactive waste and barrier materials. Appl Radiat Isot 137:177–183. https://doi.org/10.1016/j.apradiso.2018.04.008
13. Wang Z, Liu H, Lei Z, Huang L, Wu T, Liu S, Ye G, Lu Y, Wang X (2020) Graphene aerogel for photocatalysis-assist uranium elimination under visible light and air atmosphere. Chem Eng J 402:126256. https://doi.org/10.1016/j.cej.2020.126256
14. Akl ZF, Ezat A (2021) Investigation of thorium (IV) adsorptive behavior onto functionalized magnetite nanoparticles. J Radioanal Nucl Chem 328:1291–1300. https://doi.org/10.1007/s10967-021-07729-5
15. Liu T, Yuan J, Zhang B, Liu W, Lin L, Meng Y, Yin S, Liu C, Luan F (2019) Removal and recovery of uranium from groundwater using direct electrochemical reduction method: performance and implications. Environ Sci Technol 53:14612–14619. https://doi.org/10.1021/acs.est.9b06790
16. Dotto GL, McKay G (2020) Current scenario and challenges in adsorption for water treatment. J Environ Chem Eng 8:103988. https://doi.org/10.1016/j.jece.2020.103988

17. Wang J, Chen Z, Shao D, Li Y, Xu Z, Cheng C, Asiri AM, Marwani MH, Hu S (2017) Adsorption of U(VI) on bentonite in simulation environmental conditions. J Mol Liq 242:678–684. https://doi.org/10.1016/j.molliq.2017.07.048
18. Bilal M, Ihsanullah I, Younas M, Shah MU (2021) Recent advances in applications of low-cost adsorbents for the removal of heavy metals from water: a critical review. Sep Purif Technol 278:119510. https://doi.org/10.1016/j.seppur.2021.119510
19. Ma F, Gui Y, Liu P, Xue Y, Song W (2020) Functional fibrous materials-based adsorbents for uranium adsorption and environmental remediation. Chem Eng J 390:124597. https://doi.org/10.1016/j.cej.2020.124597
20. Bai J, Ma X, Yan H, Zhu J, Wang K, Wang J (2020) A novel functional porous organic polymer for the removal of uranium from wastewater. Microp Mesop Mater 306:110441. https://doi.org/10.1016/j.micromeso.2020.110441
21. Yang Z, Chen G, Weng H, Shen W, Huang Z, Lin M (2020) Efficient and selective separation of U(VI) and Th(IV) from rare earths using functionalized hierarchically mesoporous silica. J Mater Sci 53:3398–3416. https://doi.org/10.1007/s10853-017-1808-9
22. Jiang D, Liu L, Pan N, Yang F, Li S, Wang R, Wyman IW, Jin Y, Xia C (2015) The separation of Th(IV)/U(VI) via selective complexation with graphene oxide. Chem Eng J 271:147–154. https://doi.org/10.1016/j.cej.2015.02.066
23. Salah BA, Gaber MS, Kandil AT (2019) The removal of uranium and thorium from their aqueous solutions by 8-hydroxyquinoline immobilized bentonite. Minerals 9:626. https://doi.org/10.3390/min9100626
24. Ang KL, Li D, Nikoloski AN (2017) The effectiveness of ion exchange resins in separating uranium and thorium from rare earth elements in acidic aqueous sulfate media. Part 1. Anionic and cationic resins. Hydrometallurgy 174:147–155. https://doi.org/10.1016/j.hydromet.2017.10.011
25. Dacrory S, Haggag EA, Masoud AM, Abdo SM, Eliwa AA, Kamel S (2020) Innovative synthesis of modified cellulose derivative as a uranium adsorbent from carbonate solutions of radioactive deposits. Cellulose 27:7093–7108. https://doi.org/10.1007/s10570-020-03272-w
26. Alqadami AA, Naushad Mu, Alothman ZA, Ghfar AA (2017) Novel metal–organic framework (MOF) based composite material for the sequestration of U(VI) and Th(IV) metal ions from aqueous environment. ACS Appl Mater Interfaces 9:36026–36037. https://doi.org/10.1021/acsami.7b10768
27. Zhou L, Jia Y, Peng J, Liu Z, Al-Zaini E (2014) Competitive adsorption of uranium(VI) and thorium(IV) ions from aqueous solution using triphosphate-crosslinked magnetic chitosan resins. J Radioanal Nucl Chem 302:331–340. https://doi.org/10.1007/s10967-014-3125-y
28. Annam S, Rao CVSB, Sivaraman N, Sivaramakrishna A, Vijayakrishna K (2018) Carbamoylmethylphosphine oxide functionalised porous crosslinked polymers towards sequential separation of uranium (VI) and thorium (IV). React Funct Polym 131:203–210. https://doi.org/10.1016/j.reactfunctpolym.2018.07.026
29. Ladshaw AP, Wiechert AI, Das S, Yiacoumi S, Tsouris C (2017) amidoxime polymers for uranium adsorption: Influence of comonomers and temperature. Materials 10:1268. https://doi.org/10.3390/ma10111268
30. Wang CZ, Lan JH, Wu QY, Luo Q, Zhao YL, Wang XK, Chai ZK, Shi WQ (2014) Theoretical insights on the interaction of uranium with amidoxime and carboxyl groups. Inorg Chem 53:9466–9476. https://doi.org/10.1021/ic500202g
31. Rohwer H, Rheeder N, Hosten E (1997) Interactions of uranium and thorium with arsenazo III in an aqueous medium. Anal Chim Acta 341:263–268
32. Akl ZF (2021) Theoretical and experimental studies on uranium(vi) adsorption using phosphine oxide-coated magnetic nanoadsorbent. RSC Adv 11:39233–39244. https://doi.org/10.1039/D1RA04515F
33. Ao J, Zhang H, Xu X, Yao F, Ma L, Zhang L, Ye B, Li Q, Xu L, Ma H (2019) A novel ion-imprinted amidoxime-functionalized UHMWPE fiber based on radiation-induced crosslinking for selective adsorption of uranium. RSC Adv 9:28588–28597. https://doi.org/10.1039/C9RA05440E
34. Chavda HV, Patel RD, Modhia IP, Patel CN (2012) Preparation and characterization of superporous hydrogel based on different polymers. Int J Pharm Investig 2:134–139. https://doi.org/10.4103/2230-973X.104396
35. Erkartal M, Usta H, Citir M, Sen U (2016) Proton conducting poly (vinyl alcohol)(PVA)/poly (2-acrylamido-2-methylpropane sulfonic acid)(PAMPS)/zeolitic imidazolate framework (ZIF) ternary composite membrane. J Membrane Sci 499:156–163. https://doi.org/10.1016/j.memsci.2015.10.032
36. Limparyoon N, Seetapan N, Kiatkamjornwong S (2011) Acrylamide/2-acrylamido-2-methylpropane sulfonic acid and associated sodium salt superabsorbent copolymer nanocomposites with mica as fire retardants. Polym Degrad Stab 96:1054–1063. https://doi.org/10.1016/j.polymdegradstab.2011.03.012
37. Nekhunguni PM, Tavengwa NT, Tutu H (2017) Sorption of uranium(VI) onto hydrous ferric oxide-modified zeolite: Assessment of the effect of pH, contact time, temperature, selected cations and anions on sorbent interactions. J Environ Manage 204:571–582. https://doi.org/10.1016/j.jenvman.2017.09.034
38. Hu K, Liu Z, Xiu T, Zhou L, Wang Y (2020) Removal of thorium from aqueous solution by adsorption with $Cu_3(BTC)_2$ J Radioanal Nucl Chem 326:185–192. https://doi.org/10.1007/s10967-020-07310-6
39. Ali AE (2012) Removal of heavy metals from model wastewater by using carboxymehyl cellulose/2-acrylamido-2-methyl propane sulfonic acid hydrogels. J Appl Polym Sci 123:763–769. https://doi.org/10.1002/app.34470
40. Zhao Y, Li J, Zhang S, Chen H, Shao D (2013) Efficient enrichment of uranium(vi) on amidoximated magnetite/graphene oxide composites. RSC Adv 3:18952–18959. https://doi.org/10.1039/C3RA42236D
41. Afjeh MS, Marandi GB, Zohuriaan-Mehr MJ (2020) Hydrogel-rice husk biochar composite as an adsorbent for the removal of phenol and PNP from aqueous solutions. Sep Sci Technol 56:195–1210. https://doi.org/10.1080/01496395.2020.1775254
42. Song S, Liu Z, Zhang J, Jiao C, Ding L, Yang S (2020) Synthesis and adsorption properties of novel bacterial cellulose/graphene oxide/attapulgite materials for Cu and Pb ions in aqueous solutions. Materials 13:3703. https://doi.org/10.3390/ma13173703
43. Surikumaran H, Mohamad S, Sarih NM (2014) Molecular imprinted polymer of methacrylic acid functionalised β-Cyclodextrin for selective removal of 2,4-dichlorophenol. Int J Mol Sci 15:6111–6136. https://doi.org/10.3390/ijms15046111
44. Liu Z, Sun Y, Xu X, Qu J, Qu B (2020) Adsorption of Hg(II) in an aqueous solution by activated carbon prepared from rice husk using KOH activation. ACS Omega 5:29231–29242. https://doi.org/10.1021/acsomega.0c03992
45. Öztürk T, Gülfen M, Özdemir A (2020) Sorption of Pt(IV) ions on poly(m-aminobenzoic acid) chelating polymer: Equilibrium, kinetic and thermodynamic studies. SN Appl Sci 2:1886. https://doi.org/10.1007/s42452-020-03692-0

Publisher's Note Springer Nature remains neutral with regard to jurisdictional claims in published maps and institutional affiliations.